AADE-18-FTCE-SPP-05

A New Experimental Analysis of Fracture Mechanism in Sandstones using Micro-Level Observation and Digital Image Correlation

Wenhao He, Asadollah Hayatdavoudi, Kaustubh Sawant, University of Louisiana at Lafayette; Keyong Chen, Chengdu University of Technology

Abstract

Over the drilling process, one most important consideration is not to induce new fractures to keep the stability and integrity of the wellbore wall. However, the fracture mechanisms are still not convincing on (1) the fracturing process from initiation to termination, and (2) the effects of clay content and mineral distribution characteristics on the failure strength and deformability of brittle rocks. In this paper, a new experimental method of fracture mechanism analysis was proposed herein, based on a combination of a micro-level observation and digital image correlation (DIC).

Parallel to Brazilian test, a high-speed photography system was used to capture the specimen images until the rock failed. Then, all the images were processed by the DIC technique and showed a dynamic fracturing process from fracture initiation to its termination by displacement contours. On the other hand, the microscopic observation of the quartz-clay framework was performed by scanning electron microscope (SEM), X-ray diffraction (XRD) analysis, and electron-dispersive system (EDS). According to the micro-level observation, the clay content usually affected the rock strength with the clay mineral distribution characteristics. Meanwhile, three basic fracture modes (Mode Ⅰ/Ⅱ/Ⅲ) can also be distinguished through (1) the grain size, and (2) the grain shape and uniformity. Finally, two fracturing mechanisms were found: (1) the grain sliding effect through clay-cements and soft pore-fillings, and (2) the grain stick-slip effect across silica cements and strong grains. Besides, graphite was proved to be an efficient plastering material.

Introduction

Over the drilling process, there are two well-known problems related to the integrity and stability of the wellbore wall: (1) the water adsorption referring to the crystalline swelling and the surface hydration of clay-rich zones, and (2) the lost circulation into the natural and induced fractures. Both these problems can result in the difficulties in the drilling and production of the oil and gas wells[1]. To maintain a stable wellbore, many researches and studies have made great contribution in wellbore strength analysis by analytical solutions, numerical simulations, and experimental tests[1-4]. Nowadays, most of the current theoretical mechanisms are based on the principles of Griffith's Brittle Fracture Theory and the fracture toughness proposed by Irwin[2,5].

As for the clay effect on the rock strength, most of the available literatures have shown that only a small amount of clay content (1 vol.%) can reduce the rock strength significantly[6-8]. However, a high clay content did not always lead to a low rock strength[7]. Since the clays usually have complicated structures, the rock mechanical properties can get affected through the mineral composition, the amount, the extent of hydration, and location of clays the inside the rock matrix[9]. Based on the available literatures, the clay mainly affects the rock strength by the following mechanisms: (1) The clay content can directly reduce the friction resistance of the rock by reducing the grain contacts of the original interconnected quartz grains[8]. (2) The swelling effect has been proved a most important factor to reduce the grain contacts inside the well-consolidated sandstones but increase the grain compaction inside the poorly-consolidated sandstones[6,9]. (3) The clay-cement and coating, attached to the framework of grains, can help improve the material resistance, and the compression, tensile and shear stresses greatly, by contributing to binding the grains[10-12]. (4) The rock strength can also get affected by the couple of chemical corrosion deterioration and osmotic flows due to the chemical potential and reactions[13-14]. This mechanism contributes to the mineralogic changes, thus resulting in the changes of the mechanical properties.

Since the tensile strength of rock material is about 1/10 of the compressive strength, the tensile failure strength was often tested as an indicator of rock strength[15]. When it comes to the measurement of tensile strength, Brazilian test is preferred in laboratory tests due to its simplicity and efficiency[2]. In a Brazilian test, a disc-shaped specimen is mounted and loaded diametrically at the top and the bottom. However, the accuracy of the tensile strength measurements is usually affected by the compression effect near loading points, the loading angle to the

core center, and the material properties[2,16,17]. The ideal tensile failure patterns should be a fracture which is initiated at the planar center of an isotropic brittle material[2,17]. To describe the failure patterns of the tested specimen, three basic modes can be identified as shown in **Fig. 1**[5]. Among three kinds of fracture modes, Mode I indicates a tensile failure which is dominant failure mode under Brazilian test, and it usually shows up with a shear fracture Mode II, or a bending fracture Mode III. To quantify the fracture toughness of each kind of fracture mode, the International Society for Rock Mechanics have established various standard testing methods.

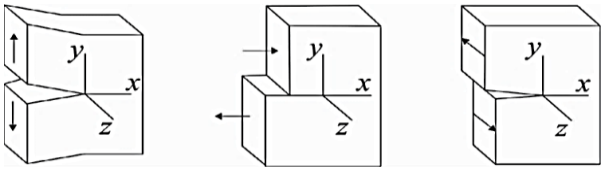

(a) Mode I (opening) (b) Mode II (sliding) (c) Mode III (tearing)

Fig.1 Schematic of three basic fracture modes[5]

Along with the development of technique advances, many researches have been conducted on microscopic observations. As a common geometry observation method, the scanning electron microscope (SEM) has been widely applied in the micro-level observation of rock microstructures, such as the grain size distribution, the geometries of the grain and the pore-fillings and pore throat[8,10-12]. Normally attached to the SEM equipment, X-Ray diffraction (XRD) and Energy-Dispersive system (EDS) can help to identify the mineral composition and the elemental distribution[8,10-11]. Moreover, thanks to the rapid development of the high-resolution cameras and computational technologies, a digital image correlation (DIC) technique has been developed and utilized to measure the displacement contours over the strength measurement process of concrete, refractories and ceramics[18-20].

Until now, many useful information can be found for the evaluation of the rock mechanical properties. However, there are still some confusions related to fracture mechanisms. Since a fracture is created all of a sudden, traditional experimental results only show the readers the final crack patterns but exhibit no evidence of the initiation and propagation of a fracture. As for the simulation results and the analytical solutions, they are only meaningful when the basic assumptions are verified. In other words, the readers cannot be fully convinced if there is a mistake in the initial inputs. Moreover, as an important indicator for the drilling safety, it is necessary to figure out the overall clay effects on the wellbore integrity. In order to further investigate the fracture mechanisms over the drilling process, this paper attempts to gap the bridge between the microscopic and continuum approaches related to rock mechanics. Firstly, we can show a dynamic fracture propagation process using DIC. To describe the micro-level observation results, SEM, XRD, and EDS will present the fracture characteristics and the effects of clay content and mineral distribution characteristics on the rock strength. After a comprehensive discussion, all the key findings will be summarized in the conclusion section.

Experimental Procedure

In this section, the overall experimental analysis procedure will be demonstrated in detail, thus helping the readers to understand the experimental data.

Sample Preparation

Considering the clay effects on the mechanical properties of brittle rocks, two kinds of sandstones are selected, due to a clay content contrast, as the Bandera Brown sandstone (BBS) and the Michigan sandstone (MS). BBS is famous for a high clay content and a high probability to swell in the presence of water while MS is distinguishable for its larger grain size and a relatively clean framework of a low clay content.

Prepared for the Brazilian test, total 18 specimens were cut into disc-shaped specimens in a same diameter of 2 inches but in variant lengths of 0.25, 0.50, 0.625, and 1.0 inches, 9 specimens for each sandstone. To mimic the changes of the rock strength, we applied three environmental effects. Among those 9 specimens, we dried a specimen of 0.625-length in an oven under a temperature of 200 ℉ for 10 minutes, saturated 4 specimens of invariant sizes with the local tap water for 24 hours, and filtrated the rest 4 specimens of invariant sizes under a pressure differential of 100 psi for 1.5 hours, in a uniaxial dynamic filter apparatus using a water-based mud with plastering materials inside.

Brazilian Test

To quantify the rock strength, we chose Brazilian test to measure the splitting tensile strength. In the experiment, the main setup of the equipment was shown in **Fig.2**. To minimize the compression effect near the loading positions, we used two special strips designed with a smooth curvature of the same radius with the specimens. By adjusting the operational parameters, i.e. the loading rate, the ending criteria, and the capture speed of images, we can record all the related data in the control system. The loading didn't stop until the rock failed and a crack showed up.

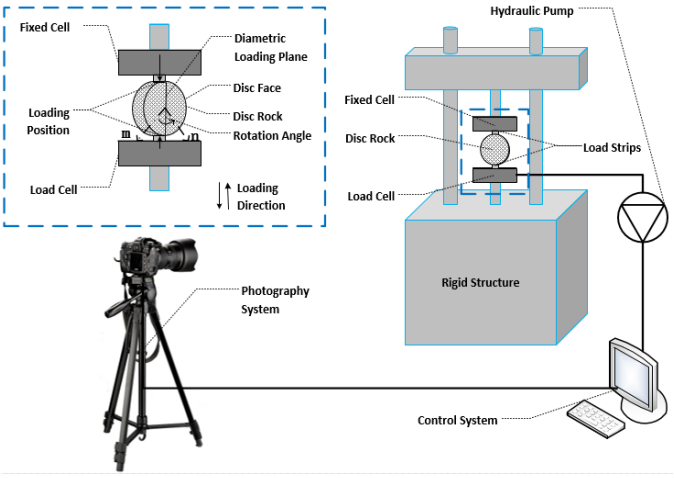

Fig.2 The equipment setup of Brazilian test

Digital Image Correlation

Over the loading process, a high-speed photography system was used to keep snapping images. Unlike the other studies, to observe the displacements in a 3D condition, we set up the normal direction of the tested specimen face, ***n***, at a 45-degree angle to the camera through a counter-clockwise rotation, as shown in **Fig.2** by the **m** direction. Thus, we can obtain the displacements beyond the disc face, which were hardly discussed in the previous studies. After the rock failed, all the captures were processed using DIC analysis tool for displacement contours. Thus, we can get a stress distribution contours since the displacement was a result and reflection of the stress. After the correlation was done, a dynamic fracturing process presented the fracture initiation, propagation and its termination. Thus, the readers can figure out the visualized fracture process.

Micro-Level Observation

After the rock failed, we can got different failure patterns. Considering the classification on basic fracture modes, we renamed them for a better understanding. As shown in **Fig. 3**, we named Mode I fracture as the friction fracture and the principle fracture due to a tensile failure while Mode III fracture was distinguished as the torsion fracture due to an obvious bending effect. As for the shear failure, Mode II fractures, the very front part was renamed as the shear lip fracture while the major part was called as shear slippage fracture. In accordance with the failure classifications, we can do specific micro-level observations due to the various fracture modes. For example, the grain size and the grain roundness can be measured by SEM.

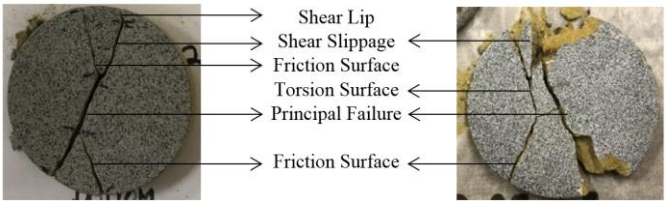

Fig.3 Failure Classifications based on Fracture Modes

To see the effects of clay content and mineral distribution characteristics on the rock deformability, XRD and EDS were also used to measure the mineral compositions and the elemental distributions.

Mechanical Test Results

Using the recorded data, the maximum load over the loading process was used to calculate the splitting tensile strength of the specimen as follow:

$$\sigma_t = \frac{2P}{\pi DL} \qquad (A.1)$$

where P was the maximum load, D is the diameter of the disc-shaped specimen, and L is the thickness of the sample. Thus, we can get the splitting tensile strengths in **Table 1**. For instance, the average splitting tensile strength was 360 psi of the water saturated Michigan sandstone (WSMS). Determine the average of the splitting tensile strengths under the same condition as the tested tensile strength of the same condition. According to the testing results, under all three conditions, MS had much higher tensile strength than BBS. Though the different specimen size resulted in a significant disparity on strength measurements, 0.625-inch-length specimen tended to exhibit a highest strength measurement. Compared with the strength of the dried ones, both the water-saturated and the mud-filtrated specimens resulted in stress losses, especially for a high stress loss under a water saturation condition. However, the testing data showed the mud filtration condition tended to cure the strength loss in the mud filtrated Michigan sandstone (MFMS), but showed no or even lower improvement in tensile resistance in the mud filtrated Bandera Brown sandstones (MFBBS) when compared with the water saturated Bandera Brown sandstones (WSBBS).

Table.1 Splitting Tensile Strength Measurements

Sample	Treatment	L, inch	P, psi	σ_t, psi	$\overline{\sigma_t}$, psi
BBS	Drying	0.625	585.43	298.16	298.16
	Water Saturation	0.25	92.82	118.18	179.81
		0.5	338.90	215.75	
		0.625	441.08	224.64	
		1	504.79	160.68	
	Mud Filtration	0.25	56.57	72.03	147.46
		0.5	265.20	168.83	
		0.625	343.93	175.16	
		1	546.07	173.82	
MS	Drying	0.625	1083.48	551.82	551.82
	Water Saturation	0.25	380.16	484.04	360.24
		0.5	257.33	163.82	
		0.625	740.53	377.15	
		1	1306.68	415.93	
	Mud Filtration	0.25	313.52	399.19	443.55
		0.5	578.12	368.04	
		0.625	1020.80	519.89	
		1	1530.18	487.07	

Dynamic Fracturing Process

As discussed before, the mass properties can get changed due to the environmental effects and the operational parameters, i.e. water saturation, mud filtration, surface smoothness. Thus, it's hard to determine the isotropy and homogeneity of the tested specimens, which is much concerned with the fracture initiation and propagation in the proposed theories. Using DIC technique, we can have a better idea about the fracture process.

In the DIC analysis, we set the 1.0-inch-thick WSBBS and the WSMS of the same size as the benchmarks due to their ideal fracture process. As shown in **Fig.4**, given the scale legend of the lateral strain, red values mean positive tension displacements while blue colors represent the negative displacements caused by the compression tests. In the middle, green values indicate no displacements. Thus, in the dynamic fracturing process shown in Fig.4, ten representative captures were shown in an increasing sequence of the loading time. As the time increased, the initial status was disturbed and different parts responded in various manners. But a biggest tension displacement accumulated near the disc center. Finally, when it reached to time T_7, a Mode I fracture showed up in the planar center and propagated along the diametrical loading plane due to a tensile failure. With a continuous loading, a secondary shear crack Mode II fracture occurred near the loading points.

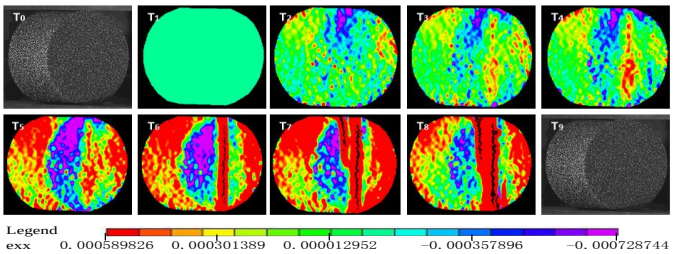

Fig.4 Dynamic Fracturing Process of 1.0-inch-thick WSBBS

During the DIC process, we also identified some other fracturing patterns as shown in **Fig.5** and **Fig.6**. In Fig.5, the fracture was initiated at the disc center due to a tensile failure. However, it propagated out of the principle fracture plane due to a bending effect. Meanwhile, regardless of a tensile failure, the failure in Fig.6 was mainly caused by a shear effect and initiated near the loading points.

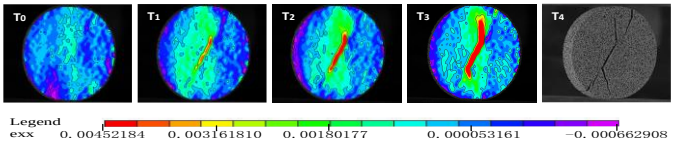

Fig.5 Dynamic Fracturing Process of 0.25-inch-thick WSBBS

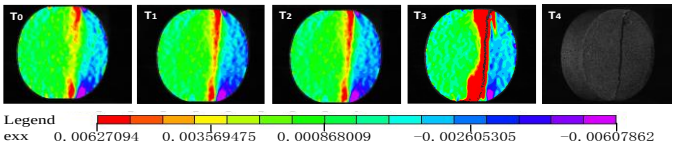

Fig.6 Dynamic Fracturing Process of 0.50-inch-thick MFBBS

According to the dynamic fracturing process, we can divide the tensile strength measurement data into three sub-groups: (1) the validate tensile failure whose fracture initiated near the center and propagated diametrically, (2) the splitting tensile strength caused by a shear failure and initiating from the loading points, and (3) the splitting tensile strength caused by a bending effect and propagating out of a plane. As a result, we finally verified the accuracy of the splitting tensile strength measurement and found the true values in **Table 2**.

Table.2 Tensile Strength Measurement after Correction

Sample	Treatment	L (inches)	P (psi)	σ (psi)	$\bar{\sigma}$ (psi)	Strength loss (%)
Bandera Brown Sandstone	Dried	0.625	585.43	298.16	298.16	0
	Water-Saturated	1	504.79	160.68	160.68	46.1
	Mud-Filtrated	0.625	343.93	175.16	175.16	41.3
Michigan Sandstone	Dried	0.625	1083.48	551.82	551.82	0
	Water-Saturated	0.625 1	779.80 1306.68	377.15 415.93	396.54	28.1
	Mud-Filtrated	0.625	1020.80	519.89	519.89	5.8

As the failure patterns showed, Mode I fractures were usually found with Mode II fractures while Mode III tended to occur in 0.25-inch-length discs, using BBS specimens, and under the mud filtration condition. In addition, a displacement along the length was also identified. When a fracture showed up, the stress concentration along the length was much similar with the right side of the disc faces, which was hardly discussed in the previous studies of 2-D planar displacements.

Micro-Level Observation Analysis

Well-known for a non-conductive testing method, the microscopic observation usually does no damages to the tested specimens. Due to a specific investigation area, only a small piece can meet a satisfactory test. In this section, we will discuss the grain size, grain roundness, clay mineral distribution and other fracture characteristics of various fracture planes.

Grain Size Distribution

Based on a direct measurement on a total collection of 640 random particles, we obtained the average grain size of each type of fracture plane as shown in **Table 3**. For example, BBS was proved to have a much smaller grain size than MS, a ratio of 132 μm to 325 μm under the dried condition. Given a Type I error of 5%, we constructed 95% confidence intervals for all the investigated fracture planes. Both the torsion surface and the tension surface exhibited much smaller grain size than the original dried grains. As for the grain sizes along the shear surface, the shear lip tended to produce slightly smaller grains than the shear slippage grains.

Table 3 Grain Size Distribution

Sample	Treatment	Specimen Sources		Fracture	Mean	SE Mean	95% CI
BBS	Original Grain	BB-Grains		Particle	132.20	1.73	(128.80,135.58)
	Water Saturation	Resistant Friction Surface		Mode Ⅰ	113.91	3.23	(107.57,120.25)
		Shear Surface	Shear lip	Mode Ⅱ	123.56	4.65	(114.44,132.68)
			Shear Slippage	Mode Ⅱ	128.38	5.09	(118.41,138.36)
	Mud Filtration	Shear Slippage Surface		Mode Ⅱ	111.90	2.32	(107.35,116.44)
		Torsion Surface		Mode Ⅲ	103.84	2.09	(99.74 ,107.94)
MS	Original Grain	M-Grains		Particle	324.98	15.53	(294.55,355.41)
	Water Saturation	Resistant Friction Surface		Mode Ⅰ	293.85	7.36	(279.43,308.27)
		Shear Surface	Shear lip	Mode Ⅱ	302.93	11.82	(279.76,326.10)
			Shear Slippage	Mode Ⅱ	312.10	13.04	(286.55,337.65)

After the determination on the grain size, a normal distribution was plotted to show the scattering, or to say the distribution and concentration, of the data. As shown in **Fig.7**, under a same magnification of 50 times, the BBS grains seemed to be much smaller than MS grains. In addition, the MS grains was measured to cover a much wider range of the grain size from 150 μm to 530 μm.

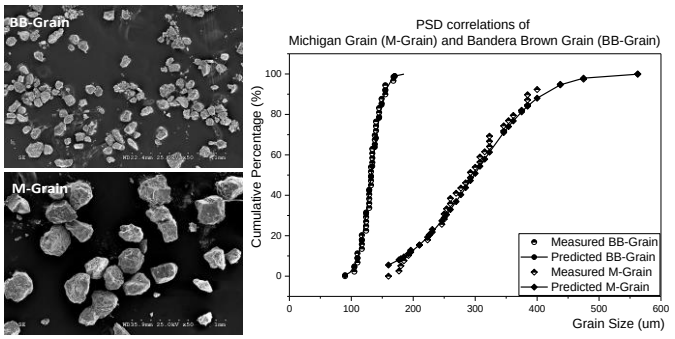

Fig.7 Grain Size Comparison between M-Grain and BB-Grain

Grain Shape Roundness

Since it's too difficult to measure the roundness and the toughness of the certain fracture, we define a new parameter as angularity factor, A-factor, which is the total number of grains with tips, jagged corners, and other angular features on the total number of grains on a certain area:

$$A_{IL} = \frac{\sum Angular + \sum Sub - Angular}{\sum Total\ Grains} \quad (A.2)$$

$$IL = 4 * AGS \quad (A.3)$$

where A_{IL} is the A-factor measured at a certain investigation length *IL* about 4 times bigger than the average grain size, and *AGS* is the average grain size. As suggested in the definition, A-factor is mainly a qualitative measurement of the roundness, which can be much efficient for a quick estimation on how well the grains are rounded using the evaluation table shown in **Table 4**, based on a box plot of 100 observations.

Table 4 Space Shape Roundness Evaluation of A-factor

A-Factor	[0,0.14]	(0.14,0.25]	(0.25,0.54]	(0.54,0.63]	(0.63,1.0]
Roundness	Well Rounded	Rounded	Sub Rounded	Poorly Rounded	Very Poorly Rounded

According to the definition of A-factor, we can obtain the roundness of the grains of certain fracture surfaces in Table 5. In contrast with a small A-factor of the friction surface, the torsion fracture Mode III had a large A-factor though it had a small grain size.

Table 5 Space Shape Roundness of Sandstones

Sample	Treatment	Surface		Fracture	A-Factor	
BBS	Original Grain	BB-Grains		Particle	0.62	
	Water Saturation	Resistant Friction Surface		Mode Ⅰ	0.14	
		Shear Surface	Shear lip	Mode Ⅱ	0.22	0.15
			Shear Slippage	Mode Ⅱ		0.32
	Mud Filtration	Shear Slippage Surface		Mode Ⅱ	0.53	
		Torsion Surface		Mode Ⅲ	0.66	
MS	Original Grain	M-Grains		Particle	0.40	
	Water Saturation	Resistant Friction Surface		Mode Ⅰ	0.32	
		Shear Surface	Shear lip	Mode Ⅱ	0.56	0.54
			Shear Slippage	Mode Ⅱ		0.58

In addition, a study of A-factor along the fracture surface characteristics was performed on a 0.25-inch-thick MFBBS in **Fig.8**, resulting in the curves presented in **Fig.9**. The arrows represented the measurement directions along the lines. A better view of undulatory terrains was presented in Fig.8(d), the left implying Fig.8(b) and the right being Fig.8(c). Since it's a qualitative measurement of the roundness, we only used the overall trend of the A-factor plot to describe the grain shape. Thus, the high A-factors from No. 15 to No. 25 in Fig. 9(a) revealed the grain roundness along the W-U section in Fig. 8(d). Another distribution of high A-factors from No.10 to No.20 in Fig.9(b) was closely related to the roundness of B-C section in Fig.8(d). Thus, a high A-factor seemed to indicate a convex along a fracture surface.

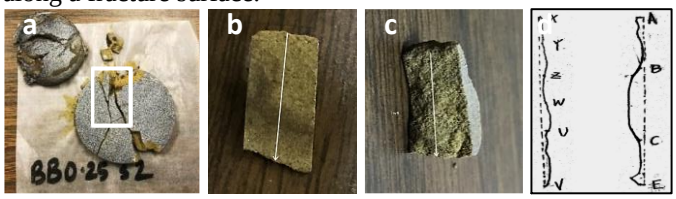

Fig.8 A-factor distributions along various fracture surfaces

To verify such a reasonable hypothesis, an A-factor distribution of the overlapping section, of the U-V section of the shear surface and the A-B section of the torsion surface in Fig.8(d), was shown in Fig.9(c) in a normalized distance. Overall, a high A-factor of one fracture surface corresponds to a low A-factor of the other fracture surface. Thus, it can be concluded that a high A-factor usually means a convex on a fracture while a low A-factor indicates a hole-like concave.

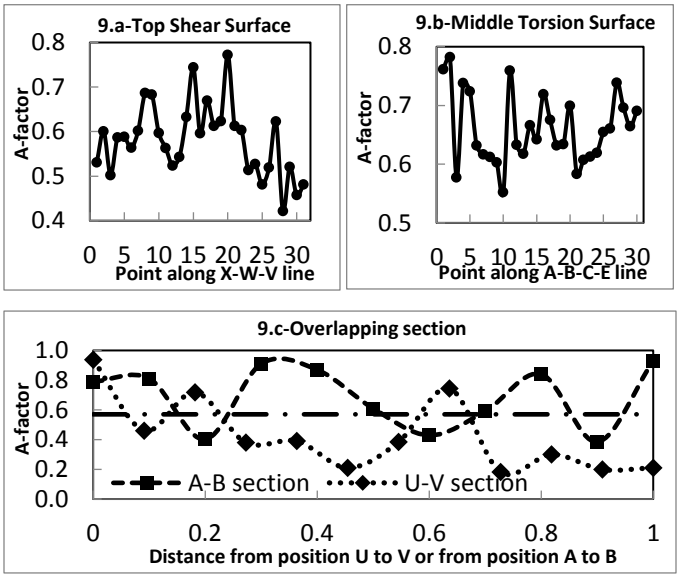

Fig.9 A-factor distributions along various fracture surfaces

Clay Content and Mineral Composition

To verify the clay content effect on the rock mechanical strength, XRD was used to test the mineral compositions of these two kinds of sandstones. In accordance with the analysis results in **Fig.10**, the Bandera Brown sandstone mainly consists a high Fe-rich clay content (Clay, 12.5 vol.%) of chlorite (Chl, 6.7 vol.%), illite (Ili, 3.3 vol.%), montmorillonite (Mtl, 2.2 vol.%), and kaolinite (Kln, 0.2 vol.%). Compared with BBS, the tested Michigan sandstone contained a much lower clay content of 5.8 vol.%. There was ignorable montmorillonite inside the MS but a relatively high content of kaolinite of 2.2 vol.%. Using the clay content theory, BS should have a lower rock strength than MS.

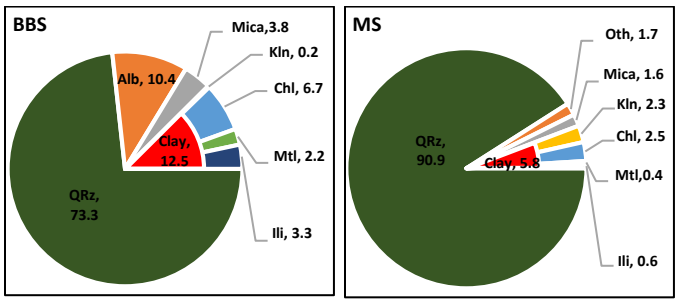

Fig. 10—Mineral composition analysis of MS and BBS

Clay Distribution Characteristics

To investigate the effect of clay distribution characteristics on the mechanical strength, we did microscopic morphologies of the quartz-clay framework and at the failure surfaces. Inside the BBS framework, the clays usually showed up in two forms of pore-fillings and chlorite cements, as shown in **Fig.11 (a)** to **Fig.11(c)**. The chlorite cement bonding (B-Chl) among grains can help to bond the loose clays and grains, contributing to a slightly increase on the mechanical strength. Meanwhile, it can also prevent grain compaction and inhibit the quartz overgrowth, thus preserving a high primary porosity. Since the clay can agglomerate at any positions and migrate with the fluid transfer in the porous media, it can fill the pores to an extent and even be cemented in situ near the pore throat. And the kind of undulatory paths also can help to an anomalous low permeability and a high water saturation inside a framework of a high log porosity in the logging analysis.

In the MS matrix, the microscopic observation presented a high probability that the kaolinite was mainly an authigenic constituent (A-Kln) of the rock and a diagenetic coating (C-Kln) to the detrital grains bonded by the silica cement (B-QRz), rather than pore-filling clays, as shown in **Fig.11(d) to Fig.11(f)**. Under a high magnification, a large number of quartz overgrowths can be identified, which helped the reduction on the primary porosity and the significant decreasing on the matrix permeability due to the aggregation near the narrow pore throats.

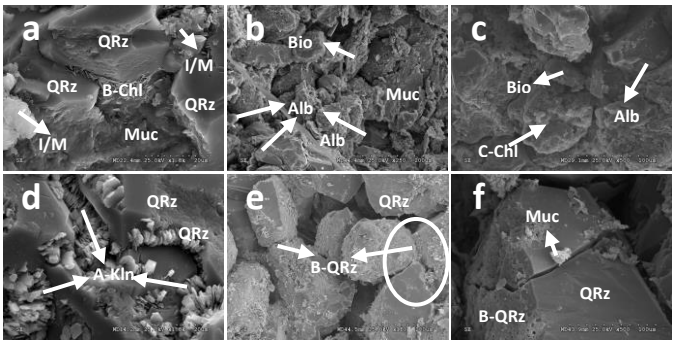

Fig.11 Clay Distribution Characteristics in BBS and MS.
Note: *QRz* for Quartz, *B-QRz* for Silica-cement bonding, *B-Chl* for Chlorite-cement bonding, *C-Chl* for Chlorite Coating, *Muc* for Muscovite, *I/M* for a mixture of Illite (*Ili*) and Muscovite (*Muc*), *Alb* for crystalline albite, *Bio* for biotite, *A-Kln* for authigenic Kaolinite.

Mineral Changes along Invasion Depth

Meanwhile, to test the chemical changes on the mineral compositions, EDS was utilized to analyze the elemental distribution along the invasion depth. Take the 1.0-inch-length MFMS specimen as an example. We measured four positions along the length, the invasion surface, the one third position, the two third position, and the bottom surface. The elemental concentration near the bottom can be considered as the original elemental compositions while the one near the top can be regarded as the zone with the most significant filtration changes.

Due to the complexity of the elemental composition, only eight significant elements were chosen for the distinguished constituent changes as shown in **Fig.12**. Along the increasing depth, Silica (Si) and Aluminum (Al) kept relatively constant. However, due to the presence of the plastering materials, Carbon (C) showed a decreasing trend when deviating from the top, being the maximum near the top. On the contrary, Oxygen (O) had an increasing concentration along with the increasing depth. Meanwhile, as for the elements with low concentrations, such as Phosphate (P), Iron (Fe), Sulphur (S) and Zinc (Zn), all of them exhibited lower and lower values when approaching the bottom.

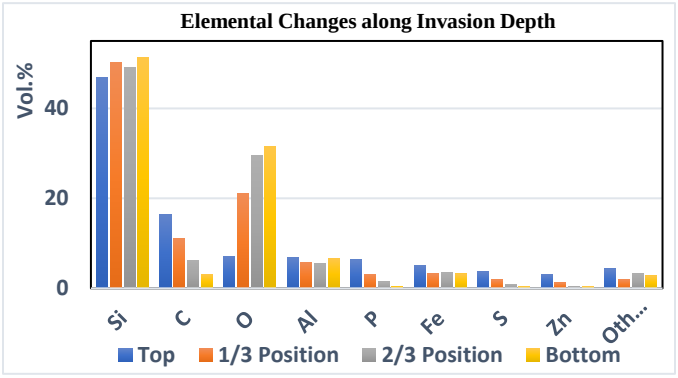

Fig.12 Mineral Compositions Along Invasion Depth

Fracture Propagation Paths

According to the microscopic observations, the fracture penetration paths showed a big difference between these two kinds of sandstones.

Along the failure plane of BS matrix, presented in **Fig.13(a)** to **Fig.13(c)**, the gains of the fracture surface were relatively intact as a whole, only with some shear damages near the grain edges, as shown in Fig.13(c). The major initiation and propagation of the fracture are across the weak chlorite cement, as shown in Fig.13(b), and the soft pore-fillings of clays, as shown in Fig.13(a), by a stable grain sliding effect.

In the Michigan sandstone, three fracture paths were identified in **Fig.13(d)** to ***Fig.13(f)*** as (1) fracture going through the silica-cement, resulting in the fracture surface, (2) fracture going through the clay coating grains, (3) fracture going through the grains cemented by quartz overgrowth. To conclude, the main direction of the fracture initiation and propagation is to fracture through strong silica-cemented grains by the stick-slip failure mechanism.

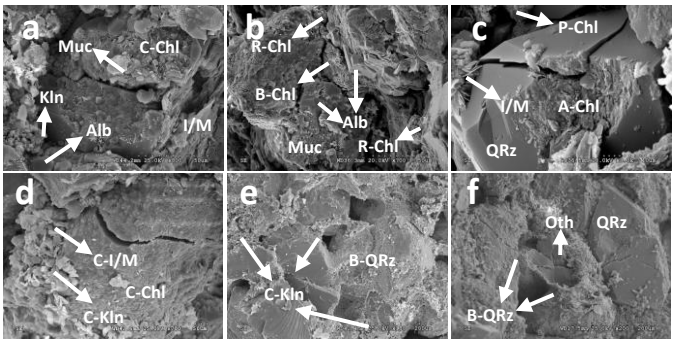

Fig.11 Fracture Propagation Paths in BBS and MS
Note: *QRz* for Quartz, *B-QRz* for Silica-cement bonding, *B-Chl* for Chlorite-cement bonding, *C-Chl* for Chlorite Coating, *R-Chl* for Rosettes of Fe-rich Chlorite, *Muc* for Muscovite, *I/M* for a mixture of Illite (*Ili*) and Muscovite (*Muc*), *Alb* for crystalline albite, *Oth* for crystalline Othoclase, *Bio* for biotite, *A-Kln* for authigenic Kaolinite, *C-Kln* for Kaolinite Coating.

Discussions

With the assistance of microscopic observations and the innovative application of digital image correlation, they helped us to comprehensively understand the fracture mechanisms in the sandstones over the drilling process.

Using the DIC technique, we can observe a dynamic fracturing process from fracture initiation to its termination, which can be used to verify the accuracy of the tensile strength measurement. In accordance with the proposed fracture theory, Brazilian test is only valid for a fracture initiating from the center and propagating along the diametrical loading plane. Only the splitting tensile strength measured under the same standard can be used for strength quantifications among tested specimens. Otherwise, the bending effect and the shear effect must be taken into consideration. Moreover, the 0.625-inch-thick disc specimens and the 0.5-inch-thick specimens were suggested to be used for the observation of the fracture initiation at the center and near the loading points, respectively. The 0.25-inch-thick MFBBS specimens can be used to observe Mode III fracture if interested.

Using XRD analysis, MS has only about 5.8 vol.% clay content, much lower than that of 12.5 vol% in BBS. Thus, using the clay content theory, MS should have a much higher splitting tensile strength, which has been verified by Brazilian Test. Due to the swelling effect of clays on the rock strength, BBS was proved to have a much higher tensile strength loss than MS with a lower clay content, being higher than 40% under both the water-saturated and the mud-filtrated conditions. On the contrary, MS had a much lower strength loss, 28% under the water-saturated condition and 5% under the mud-filtrated condition. As for the cure effect of the mud on the strength loss, we provided two explanations herein: (1). Since the mud filtration was performed with a relatively high pressure differential, the rock strength can get increased due to the slightly compaction of the grains, and (2) Due to the presence of plastering materials, the plastering effect of the strengthening materials can enhance the rock structures. Using EDS, the high elemental concentration of Carbon should come from the graphite inside the mud composition.

When it comes to the morphologies of the grains, we obtained many useful information related to the grain size, the grain shape roundness, the clay distribution, and the fracture propagation paths: (1). BBS was proved to be a fine-grained sandstone while MS had a much larger grain size on the average and a quite wider grain size distribution. (2). Among three basic fracture modes, Mode I was found to have a small grain size and a good roundness while Mode III seemed to have a small grain size but a worst roundness. Meanwhile, the initiation position of a shear fracture tended to have a slightly smaller grain size than the main shear slippage surface. (3). Based on a new definition of A-factor, a high A-factor usually mean a new fracture convex or a cornered tip along the fracture surface. (4). As for the clay distribution characteristics inside the quartz-clay framework, we found a large number of chlorite cements inside BS and lots of coated clays to the detrital grains by silica cements. (5). In the microscopic view, two different fracturing mechanisms were found. In BS matrix, the dominant fracturing propagation way was accomplished by one grain sliding effect through soft pore-filling clays and weak clay cements. On the other hand, the main fracturing path was across the silica-cemented grains by the stick-slip effect.

In the next studies, we will continue our researches further in the application of DIC and the chemical deterioration effect of clays on the rock strength. Using DIC, we can keep studying the displacement on the length and the circumference boundary constraints of the displacements under a rotated 3-D mode, due to the limited available literatures. Meanwhile, we can check the anisotropy effect on the fracture initiation and propagation for those specimens with evident natural fractures, lamination layers and interbedded rocks with various lithofacies. Another potential application of DIC on dynamic fracturing description is to analyze the fracture development in the hydraulic fracturing phase in a similar way. In addition, since a high A-factor normally means a convex on a fracture surface, it can be further investigated for the description of the roundness and the roughness of a fracture surface.

Conclusions

In this research, an innovative experimental method was proposed to help to fully explain the fracture mechanisms, especially in the understanding of a dynamic fracturing process and the overall clay effects on the rock strength. Based on a combination of the DIC technique and microscopic observations, the key findings related to two kinds of sandstones are summarized below:

(1). Digital image correlation (DIC) is a powerful tool to capture a dynamic fracturing process by analyzing the displacement contours. It can be used for the evaluation of the measurement accuracy of Brazilian Test, considering the shear effect and the bending effect. By setting the specimen in a 3-D mode, the changes beyond the disc face can be observed, and an obvious constraint boundary can be identified.

(2). Bandera Brown Sandstone is proved to be a fine-grained sandstone and has a grain size of 132 μm on the average.

Comparing the previous one, Michigan sandstone has a much larger average of grain size about 325 μm and covers a much wider grain size, being coarse-grained. As for the clay content contrast, Bandera Brown sandstone has a clay content of 12.5 vol.% while that of Michigan sandstone is only about 5.8 vol.%.

(3). A new angularity parameter, A-factor, can be used to measure the grain shape roundness qualitatively. It's a fast and efficient method to compare the roundness level. In detail, a high A-factor usually mean a new fracture convex or a cornered tip along the fracture surface.

(4). Among three basic fracture modes, Mode I fracture tends to have a small grain size and a good roundness while Mode III seems to have a small grain size but a bad roundness. As for the shear failures, Mode II fracture, the very front part near the initiation of the shear crack has a slightly smaller grain size and a slightly better roundness than those of the main shear slippage surface.

(5). On a macro level, a high clay content contributes to a low rock strength of Bandera Brown sandstone and a high strength loss over 40% when swelling. The cure effect of plastering materials on the strength loss is not significant for a high clay content but becomes much obvious for a low clay content. Meanwhile, the graphite can be a significant constituent of LCM composition.

(6). From the microscopic observations, two different cement mechanisms exist as a clay cement (i.e., the chlorite cement) in the Bandera Brown sandstone, and a silica cement in the Michigan sandstone. The presence of the clays also shows a difference between two sandstones, mainly being pore-fillings in Bandera Brown sandstone and being coated to grains in Michigan sandstones. In addition, there are two kinds of fracture mechanisms as a grain sliding effect through soft pore-filling clays and weak clay cements in Bandera Brown sandstone, and a dominant stick-slip effect to across the silica-cemented grains.

Acknowledgments

The authors would like to thank Dr. Thomas C. Pesacreta and Mr. Mike Purpera, in University of Louisiana at Lafayette, for their guidance and help on the micro-level observations. We also appreciate Mr. Kaustubh Sawant and Mr. Mathew Lomas for their help in conducting laboratory experiments.

Nomenclature

σ_t	=	the splitting strength of the rock, psi
$\overline{\sigma_t}$	=	the average splitting failure strength, psi
P	=	the maximum applied load, psi
D	=	the diameter of the specimen disc, inch
L	=	the thickness of the cylinder specimen
IL	=	the investigation length, um
AGS	=	the average grain size, um
A-factor	=	Angularity factor, dimensionless
A_{IL}	=	the *A-factor* measured at *IL*, dimensionless
Alb	=	Albite mineral
BBS	=	Bandera Brown sandstone
BB-Grain	=	Bandera Brown sandstone grain
Bio	=	Biotite
Chl	=	Chlorite clays
R-Chl	=	Chlorite rosettes
B-Chl	=	Chlorite-cement bonding by clay cement
C- Chl	=	Chlorite coating
P-Chl	=	Chlorite pore-fillings
DIC	=	Digital image correlation
Ili	=	Illite clays
I/M	=	a mixture of Illite (Ili) and Muscovite (Muc)
Kln	=	Kaolinite clays
A-Kln	=	authigenic kaolinite constituent
C-Kln	=	Kaolinite coating
MS	=	Michigan sandstone
M-Grain	=	Michigan sandstone grain
MFBBS	=	Mud Filtrated Bandera Brown sandstone
MFMS	=	Mud Filtrated Michigan sandstone
Mtl	=	Montmorillonite clays
Muc	=	Muscovite
Oth	=	Othoclase mineral
QRz	=	Quartz mineral
B-QRz	=	Silica cemented Quartz
SEM	=	Scanning Electron Microscope
vol.%	=	volume fraction
WSBBS	=	Water Saturated Bandera Brown sandstone
WSMS	=	Water Saturated Michigan sandstone

References

1. Cheatham, J. B., 1984. Wellbore Stability. *Journal of petroleum technology*, 36(06), 889-896.
2. Colback, P. S. B., 1966. An analysis of brittle fracture initiation and propagation in the Brazilian test. In 1st ISRM Congress. International Society for Rock Mechanics.
3. Steiger, R.P. and Leung, P.K. 1989. Predictions of wellbore stability in shale formations at great depth. *ISRM International Symposium*, International Society for Rock Mechanics. ISRM-IS-1989-148.
4. Wang, Bin, et al. "Lab Testing and Finite Element Method Simulation of Hole Deflector Performance for Radial Jet Drilling." *Journal of Energy Resources Technology* 139.3 (2017): 032906.
5. Wu, H., Kemeny, J., Wu, S., 2017. Experimental and numerical investigation of the punch-through shear test for mode II fracture toughness determination in rock. *Engineering Fracture Mechanics*, 184, 59-74. ISSN 0013-7944.
6. Han, D. H., Nur, A., and Morgan, D., 1986. Effects of porosity and clay content on wave velocities in sandstones. *Geophysics*, 51(11), 2093-2107.
7. Hawkins, A. B., and McConnell, B. J., 1992. Sensitivity of sandstone strength and deformability to changes in moisture content. *Quarterly Journal of Engineering Geology and Hydrogeology*, 25(2), 115-130.
8. Tembe, S., Lockner, D. A., and Wong, T. F., 2010. Effect of clay content and mineralogy on frictional sliding behavior of simulated gouges: Binary and ternary mixtures of quartz, illite, and montmorillonite. *Journal of Geophysical Research: Solid Earth*, 115(B3).
9. Jizba, D.L., 1991. Mechanical and acoustical properties of sandstones and shales. Ph.D thesis, Stanford University, USA.
10. Hosseini, M. S., and Hayatdavoudi, A., 1986. Reservoir Characterization of Tuscaloosa Sand by Mineralogical and

Petrophysical Data. Society of Petroleum Engineers. doi:10.2118/14274-PA.
11. Tudge, J., Lovell, M. A., Davies, S. J., et al., 2013. Saturation Estimates in Low Resistivity Sandstones: An Integrated Approach. Society of Petrophysicists and Well-Log Analysts. SPWLA-2013-J.
12. Ajdukiewicz, J. M., and Larese, R. E., 2012. How clay grain coats inhibit quartz cement and preserve porosity in deeply buried sandstones: Observations and experiments. *AAPG bulletin*, 96(11), 2091-2119.
13. Hale, A. H., Mody, F. K., and Salisbury, D. P., 1993. The influence of chemical potential on wellbore stability. *SPE drilling & completion*, *8*(03), 207-216.
14. Van Oort, E., Hale, A. H., and Mody, F. K., 1995. Manipulation of coupled osmotic flows for stabilisation of shales exposed to water-based drilling fluids. In *SPE Annual Technical Conference and Exhibition*. Society of Petroleum Engineers.
15. Wiid, B. L., 1970. The influence of moisture on the pre-rupture fracturing of two rock types. *International Society of Rock Mechanics, Proceedings*, 2(3-4), 239-245.
16. Sabri, M., Ghazvinian, A., Nejati, H. R., 2016. Effect of particle size heterogeneity on fracture toughness and failure mechanism of rocks. *International Journal of Rock Mechanics and Mining Sciences*, 81, 79-85.
17. Rocco, C., Guinea, G. V., Planas, J., et al., 1999. Size effect and boundary conditions in the Brazilian test: experimental verification. *Materials and Structures*, 32(3), 210-217.
18. Belrhiti, Y., Pop, I. O., 2013. The Mechanical Fracture Characterization of Non-Linear Flexible Ceramics Using Digital Image Correlation. In ICF13.
19. Ganganagoudar, A. G., Shanmugam, S. P., Gunisetty, S., 2016. A Study on Residual Compression Behavior of Structural Fiber Reinforced Concrete Exposed To Moderate Temperature Using Digital Image Correlation. *International Journal of Concrete Structures and Materials*, 10, 1–11.
20. Robert, L., Nazaret, F., Cutard, T., et al., 2007. Use of 3-D Digital Image Correlation to characterize the mechanical behavior of a Fiber Reinforced Refractory Castable. *Experimental Mechanics*, 47, 761-773.